Model Space Localization Is Not Always Better Than Observation Space Localization for Assimilation of Satellite Radiances

LILI LEI

Cooperative Institute for Research in Environmental Sciences, University of Colorado Boulder, and NOAA/Earth System Research Laboratory/Physical Sciences Division, Boulder, Colorado

JEFFREY S. WHITAKER

NOAA/Earth System Research Laboratory/Physical Sciences Division, Boulder, Colorado

(Manuscript received 16 December 2014, in final form 9 June 2015)

ABSTRACT

Covariance localization is an essential component of ensemble-based data assimilation systems for large geophysical applications with limited ensemble sizes. For integral observations like the satellite radiances, where the concepts of location or vertical distance are not well defined, vertical localization in observation space is not as straightforward as in model space. The detailed differences between model space and observation space localizations are examined using a real radiance observation. Counterintuitive analysis increments can be obtained with model space localization; the magnitude of the increment can increase and the increment can change sign when the localization scale decreases. This occurs when there are negative background-error covariances and a predominately positive forward operator. Too narrow model space localization can neglect the negative background-error covariances and result in the counterintuitive analysis increments. An idealized 1D model with integral observations and known true error covariance is then used to compare errors resulting from model space and observation space localizations. Although previous studies have suggested that observation space localization is inferior to model space localization for satellite radiances, the results from the 1D model reveal that observation space localization can have advantages over model space localization when there are negative background-error covariances. Differences between model space and observation space localizations disappear as ensemble size, observation error variance, and localization scale increase. Thus, large ensemble sizes and vertical localization length scales may be needed to more effectively assimilate radiance observations.

1. Introduction

The ensemble Kalman filter (EnKF; Evensen 1994; Burgers et al. 1998) uses a Monte Carlo approach to estimate the flow-dependent background-error covariance and combine observation information with an ensemble of forecasts. It has been widely used in atmospheric applications (e.g., Houtekamer and Mitchell 1998; Whitaker et al. 2004; Houtekamer et al. 2005; Buehner et al. 2010a,b). For large geophysical applications, EnKF assimilation systems typically use ensembles of orders 10^2. Thus, the use of the background-error covariance matrix from the direct outer product of ensemble perturbations tends to be severely rank deficient and compromised by sampling error, leading to degraded analyses and filter divergence. One treatment for the sampling error and increasing the rank of the covariance matrix is covariance localization (Houtekamer and Mitchell 1998), which limits the impact of observations on remote state variables but preserves the large and meaningful correlations close to observations. Houtekamer and Mitchell (2001) and Hamill et al. (2001) adopted the compactly supported polynomial approximation of a normal distribution given by Gaspari and Cohn (1999; GC) and demonstrated the efficacy of a distance-based localization to reduce the impact of spuriously large covariances from remote observations.

Covariance localization can be performed in the horizontal and vertical (Houtekamer et al. 2005), and in time (Anderson 2007; Chen and Oliver 2010). Moreover,

Corresponding author address: Lili Lei, NOAA/Earth System Research Laboratory/Physical Sciences Division, 325 Broadway R/PSD1, Boulder, CO 80305.
E-mail: lili.lei@noaa.gov

DOI: 10.1175/MWR-D-14-00413.1

different localizations are also preferred for different observation types (Houtekamer and Mitchell 2005) and kinds of state variable (Anderson 2007, 2012; Kang et al. 2011). Based on sample correlations, several methods have been developed to compute the localization function dynamically (e.g., Anderson 2007; Bishop and Hodyss 2009a,b; Zhou et al. 2008; Emerick and Reynolds 2011; Anderson 2012; Anderson and Lei 2013; Zhen and Zhang 2014).

Localization can be implemented as a Schur (Hadamard) product of the sample background-error covariance matrix and a positive semidefinite localization matrix (Houtekamer and Mitchell 1998), which is called model space localization. Model space localization is used in ensemble-variational data assimilation systems (e.g., Wang et al. 2008). In a serial EnKF, where observations are assimilated one by one or in batches, localization is often implemented by multiplying the sample covariance between observation and model state priors and the sample covariance between observation and observation priors by a distance-dependent function (Houtekamer and Mitchell 2001; Hamill et al. 2001), which is called observation space localization. Localization can also be implicitly implemented by applying the assimilation algorithm on local regions and with distance-dependent observation error statistics as in the local ensemble transform Kalman filter (LETKF; Ott et al. 2004; Hunt et al. 2007; Miyoshi et al. 2007).

Satellite radiances are an essential component of the global and regional assimilation systems, and their assimilation has a strong positive impact on forecast skill, especially where conventional observations are sparse (e.g., Derber and Wu 1998; Le Marshall et al. 2006; McNally et al. 2006; McCarty et al. 2009; Collard and McNally 2009). Satellite radiances are integral observations that provide information about temperature and moisture in an atmospheric column. As with other kinds of integral observations, correlations between radiances and model state variables in the column can be very different than local observations of model state variables (Anderson and Lei 2013). For this reason, vertical localization for satellite radiance observations is not as straightforward as for "conventional" observations (local observations of model state variables). This is especially true for observation space localization, since the distance between an observation and a model state variable is not a well- defined quantity. Houtekamer et al. (2005) and Houtekamer and Mitchell (2005) assimilated Advanced Microwave Sounding Unit A (AMSU-A) radiance observations by treating them as local observations whose vertical location is defined by the level at which the weighting function used in the radiative transfer peaks. Miyoshi and Sato (2007) used the flow-dependent normalized weighting function itself to define the vertical localization function. Fertig et al. (2007) proposed a localization method for assimilating radiance observations in the LETKF, where the state at a given location is updated by radiance observations that are strongly correlated to the model state. In contrast, model space localization does not involve the forward observation operator, and so the notion of a distance between model state variables and observations is not required. Campbell et al. (2010) suggested that localizing radiance observations in model space was more accurate than localizing in observation space.

The differences between model space and observation space localization is explored here using a real radiance observation. Based on the findings from the single radiance observation experiment, the performance of model space and observation space localization is compared in an idealized 1D model where the true error covariance is known. Although Campbell et al. (2010) found that observation space localization was inferior to model space localization, the results from the idealized 1D model reveal situations where the opposite can be true.

The theoretical basis for localization in model and observation space is described in section 2. Section 3 presents the single radiance observation experiment. Section 4 presents comparisons of model space and observation space localizations in an idealized 1D model. Section 5 summarizes the results and conclusions.

2. Theoretical basis for localization in model and observation space

In the context of the EnKF, the analysis increment (analysis − background) equals the Kalman gain $\mathbf{K}$ multiplied by the innovation vector that is the difference between the observation and the prior estimate of the observation. To compute the innovation vector for radiance observations, a radiative transfer model is used to convert the model state vector that includes temperature, water vapor, and other radiatively active trace gases (such as ozone) to radiance. Since the innovation vector is not affected by localization, we only focus on $\mathbf{K}$ here.

Without localization, $\mathbf{K}$ is given by (Evensen 1994)

$$\mathbf{K} = \mathbf{P}^f\mathbf{H}^{\mathrm{T}}(\mathbf{H}\mathbf{P}^f\mathbf{H}^{\mathrm{T}} + \mathbf{R})^{-1}, \tag{1}$$

where $\mathbf{P}^f$, an $n \times n$ matrix (n is number of state variables), is the sample background-error covariance matrix; $\mathbf{H}$, a $p \times n$ matrix (p is number of observations), is the forward observation operator (linearized about the background state); and $\mathbf{R}$, a $p \times p$ matrix, is the

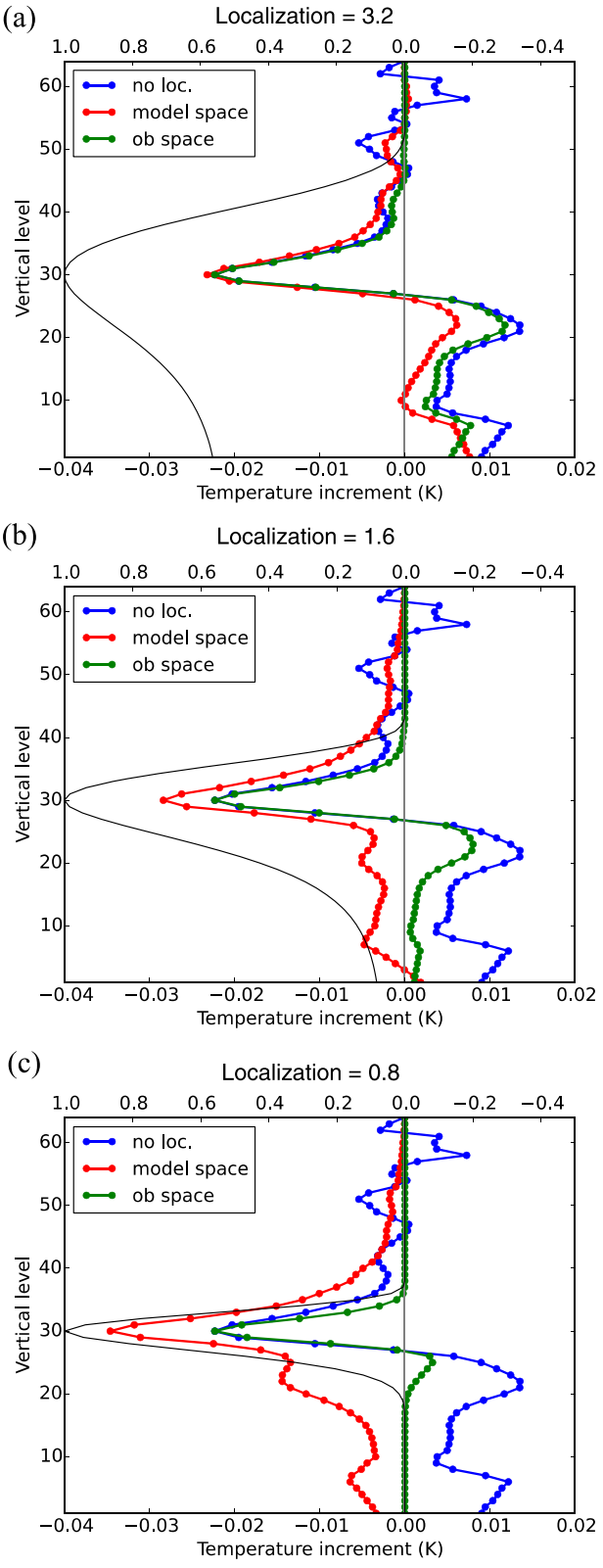

FIG. 1. Temperature increment profiles from a single radiance observation with localization scale (a) 3.2, (b) 1.6, and (c) 0.8 ln(p). The blue line indicates no localization, and red and green lines indicate localization in model and observation space, respectively. The black solid line represents the GC localization function.

observation error covariance. For satellite radiances, $\mathbf{H}$ is the Jacobian matrix, which is the partial derivative of the radiance with respect to the model state.

Following Houtekamer and Mitchell (2001), model space localization is given by

$$\mathbf{K} = (\rho_m \circ \mathbf{P}^f)\mathbf{H}^{\mathrm{T}}[\mathbf{H}(\rho_m \circ \mathbf{P}^f)\mathbf{H}^{\mathrm{T}} + \mathbf{R}]^{-1}, \quad (2)$$

where ρ_m is the covariance localization matrix in model space, and $\circ$ denotes the Schur (elementwise) product. Given a symmetric and positive semidefinite localization matrix ρ_m, the product $\rho_m \circ \mathbf{P}^f$ is a valid covariance matrix (Gaspari and Cohn 1999). With localization in observation space, $\mathbf{K}$ can be written as

$$\mathbf{K} = [\rho_{o1} \circ (\mathbf{P}^f\mathbf{H}^{\mathrm{T}})][\rho_{o2} \circ (\mathbf{H}\mathbf{P}^f\mathbf{H}^{\mathrm{T}}) + \mathbf{R}]^{-1}. \quad (3)$$

Here ρ_{o1} and ρ_{o2} are the localization matrices for observation space localization. The ρ_{o1} is an $n \times p$ matrix with each column containing the localization function for one observation with the state vector, while ρ_{o2} is a $p \times p$ matrix with each column containing the localization function for one observation with all the other observations. Localization in model space is directly applied to the background-error covariance matrix and it is conducted before operating the transpose of the forward operator; localization in observation space is operated after the forward operator multiplying the background-error covariance matrix. Because the forward operator and localization operations do not associate or commute, observation space and model space localization are not equivalent.

3. Single radiance observation experiment

To illustrate the differences of vertical localization in model and observation space, a single radiance observation experiment is conducted. A randomly chosen radiance observation from *NOAA-15* AMSU-A N15 channel 7, which is located at (80.18°S, 5.14°E) and valid at 0000 UTC 10 April 2014, is used. (Similar results are obtained for other randomly chosen observations, but not shown.) In our calculations, its vertical location is assigned to level 30 (around 280 hPa) where the weighting function peaks. The prior ensemble of temperature profiles at the assigned observation location and time are interpolated from the prior ensemble of a 6-h cycling EnKF experiment that uses the NCEP GFS with a resolution of T574L64 and 80 ensemble members. The Jacobian matrix and observation priors are computed by the Community Radiative Transfer Model (CRTM; Weng 2007; Han et al. 2007). For the particular observation and background, the innovation is negative. The temperature

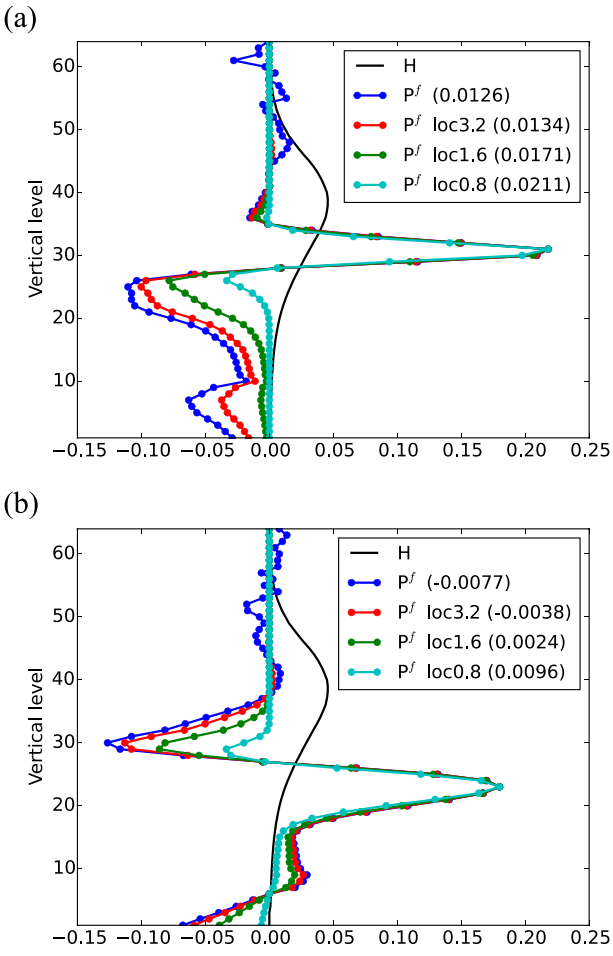

FIG. 2. Forward operator $\mathbf{H}$ for the single radiance observation, and a row of $\mathbf{P}^f$ with different localization scales for state variable temperature at level (a) 30 and (b) 22 with temperature at all levels. The value in the parentheses denotes the integral of $\mathbf{H}$ and $\rho \circ \mathbf{P}^f$ at a given level.

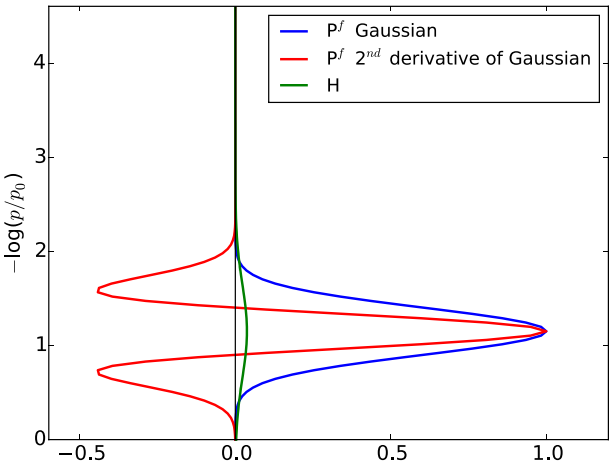

FIG. 3. True Gaussian and the second derivative of Gaussian error covariances with *e*-folding scale 0.5 for level 25 with all levels, and a forward operator for an observation with an *e*-folding scale 1.0 and a correlation peak at level 25.

increment profile is computed with GC localization in model and observation space using (2) and (3).

The blue line in Fig. 1 shows the analysis temperature increment profile without localization. Three localization scales, 3.2, 1.6, and 0.8 (in the units of natural log of pressure), are applied. With the larger localization scale (3.2), the increments around the assigned observation location from model space and observation space localizations are similar. The model space localization increment tapers to zero at larger separations than the observation space localization increment, which suggests that to be equivalent to observation space localization, model space localization requires a smaller localization scale. When the localization scale in observation space decreases, the increment around the assigned observation location stays similar, and the increments decrease away from the assigned observation location. However, when localization scale in model space decreases, the magnitude of the increment around the assigned observation location becomes larger, and the sign of increment below level 27 changes from negative to positive. Buehner et al. (2010a) showed that broader vertical localization in model space resulted in less local analysis increment, but vice versa when localizing in observation space; and a possible explanation was the neglect of negative correlations. Thus, the structure of $\mathbf{H}$ and $\mathbf{P}^f$ are examined here in order to explain the counterintuitive increments with model space localization.

Figure 2a shows $\mathbf{H}$ for this single radiance observation and the row of $\mathbf{P}^f$ at the assigned observation location (level 30). Please note that the peak level of $\mathbf{H}$ (level 40) is different from that of weighting function (level 30), because the former gives the level where the radiance observation has the largest gradient with respect to model temperature and the latter is the level where the maximal transmittance is obtained; $\mathbf{H}$ has continuously nonnegative values in the vertical. The background error covariances between temperature at level 30 and temperature below level 27 are negative. For model space localization, ρ_m is applied to $\mathbf{P}^f$ before operating on $\mathbf{H}^{\mathrm{T}}$ [(2)]; thus, as the localization scale decreases, the negative covariances are effectively neglected, and the values of $\mathbf{H}(\rho \circ \mathbf{P}^f)\mathbf{H}^{\mathrm{T}}$ and $(\rho \circ \mathbf{P}^f)\mathbf{H}^{\mathrm{T}}$ at the assigned observation location increase. For this particular observation, the magnitude of $\mathbf{H}(\rho \circ \mathbf{P}^f)\mathbf{H}^{\mathrm{T}}$ is much smaller than $\mathbf{R}$; therefore, the larger positive value from $(\rho \circ \mathbf{P}^f)\mathbf{H}^{\mathrm{T}}$ leads to a larger increment at the assigned observation location when the scale of ρ_m decreases.

To explain why the analysis increment changes sign below level 27 when the localization scale in model

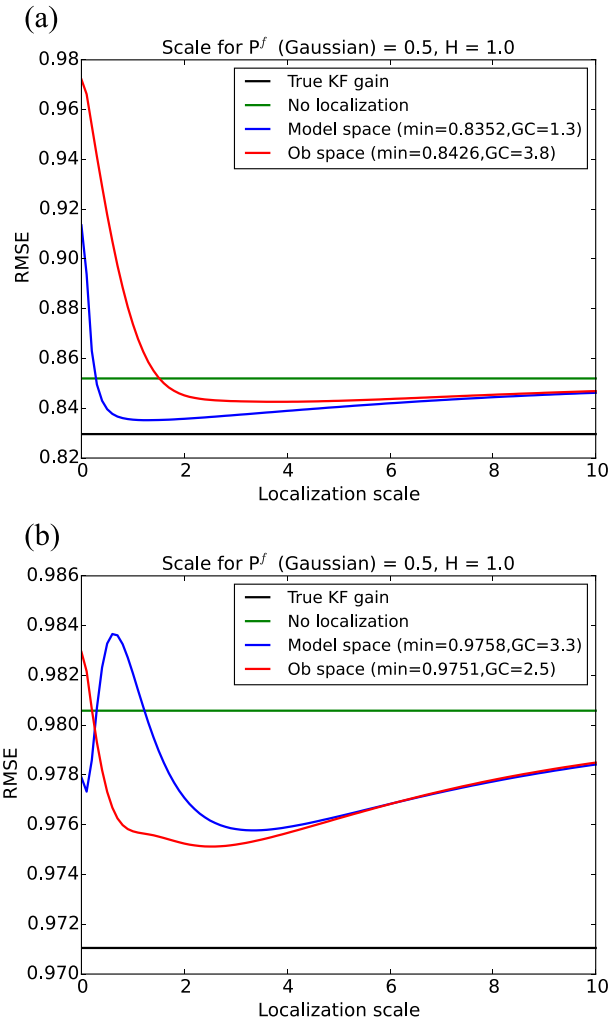

FIG. 4. Average analysis RMSE with different localization scales when the true covariance is (a) Gaussian and (b) the second derivative of a Gaussian, given that the length scale for the true covariance is 0.5, the length scale of the forward operator is 1.0, the observation error variance is 0.1, and it has an ensemble size of 40. The black solid line denotes the average analysis RMSE using the true Kalman gain, and the green solid line presents the average analysis RMSE using the estimated Kalman gain without localization.

space decreases, the analysis increment at level 22 is analyzed as an example. The row of $\mathbf{P}^f$ at level 22 with different model space localization scales is shown in Fig. 2b. The covariance is positive around level 22, and it becomes negative between levels 26 and 30. The analysis increment with model space localization is proportional to $(\rho \circ \mathbf{P}^f)\mathbf{H}^{\mathrm{T}}$ [(2)], and the innovation is negative. With broad localization, $(\rho \circ \mathbf{P}^f)\mathbf{H}^{\mathrm{T}}$ at level 22 is negative, which produces a positive increment at level 22. When the localization becomes narrower, the negative covariances between levels 26 and 30 are effectively eliminated, and $(\rho \circ \mathbf{P}^f)\mathbf{H}^{\mathrm{T}}$ at level 22 becomes positive. Thus, a negative increment is produced and the analysis increment changes sign with small localization scale in model space.

4. Idealized 1D model

Section 3 illustrated the differences between model space and observation space localizations for a real radiance observation, but the performance from different localizations cannot be validated, since the true Kalman gain $\mathbf{K}$ is unknown. To evaluate the relative performance of model space and observation space localizations, an idealized 1D model is used here. The idealized 1D model has 101 equally distributed vertical levels between 1000 and 10 hPa with interval 0.046 units of $-\ln(p/p_s)$, where p_s is the surface pressure. The true state values are assumed to be 0 for all levels. Two kinds of true error covariance are used: one is Gaussian (without negative correlations) and the other is the second derivative of Gaussian (with negative correlations). With an e-folding scale of 0.5 (the default value), the two kinds of true error covariances for level 25 (around 316 hPa) are shown by the blue and red lines in Fig. 3. The forward operator $\mathbf{H}$ is simply a vertical average with Gaussian kernel. The green line in Fig. 3 shows the $\mathbf{H}$ that peaks at level 25 with an e-folding scale 1.0 (the default value). Three observations that have $\mathbf{H}$ peaking at levels 25, 50, and 75 are generated by adding random draws from a normal distribution with mean 0 and specified $\mathbf{R}$ to the true observation value. The default value for $\mathbf{R}$ is set to 0.1. The sample error covariance is obtained by randomly sampling the true error covariance, and the default ensemble size is 40. The GC function is used for localization in model and observation space. The sample $\mathbf{K}$ is computed with localization in model and observation space, and an analysis is produced with the sample $\mathbf{K}$. The root-mean-square error (RMSE) of the analysis relative to the true state value is calculated and averaged over 10 000 trials.

Figure 4 shows the RMSE with different localization scales given the default parameters. When the true covariance is Gaussian, model space localization always performs better than observation space localization with localization scales smaller than 7.0 [as was shown by Campbell et al. (2010)]. The minimum error with model space localization is 0.8352 at a localization scale 1.3, while the minimum error with observation space localization is 0.8426 at a localization scale 3.8. When the true covariance is the second derivative of Gaussian and contains significant negative values, observation space localization is better than model space localization for localization scales between 0.2 and 5.0. Observation space localization obtains the minimum error 0.9751 at

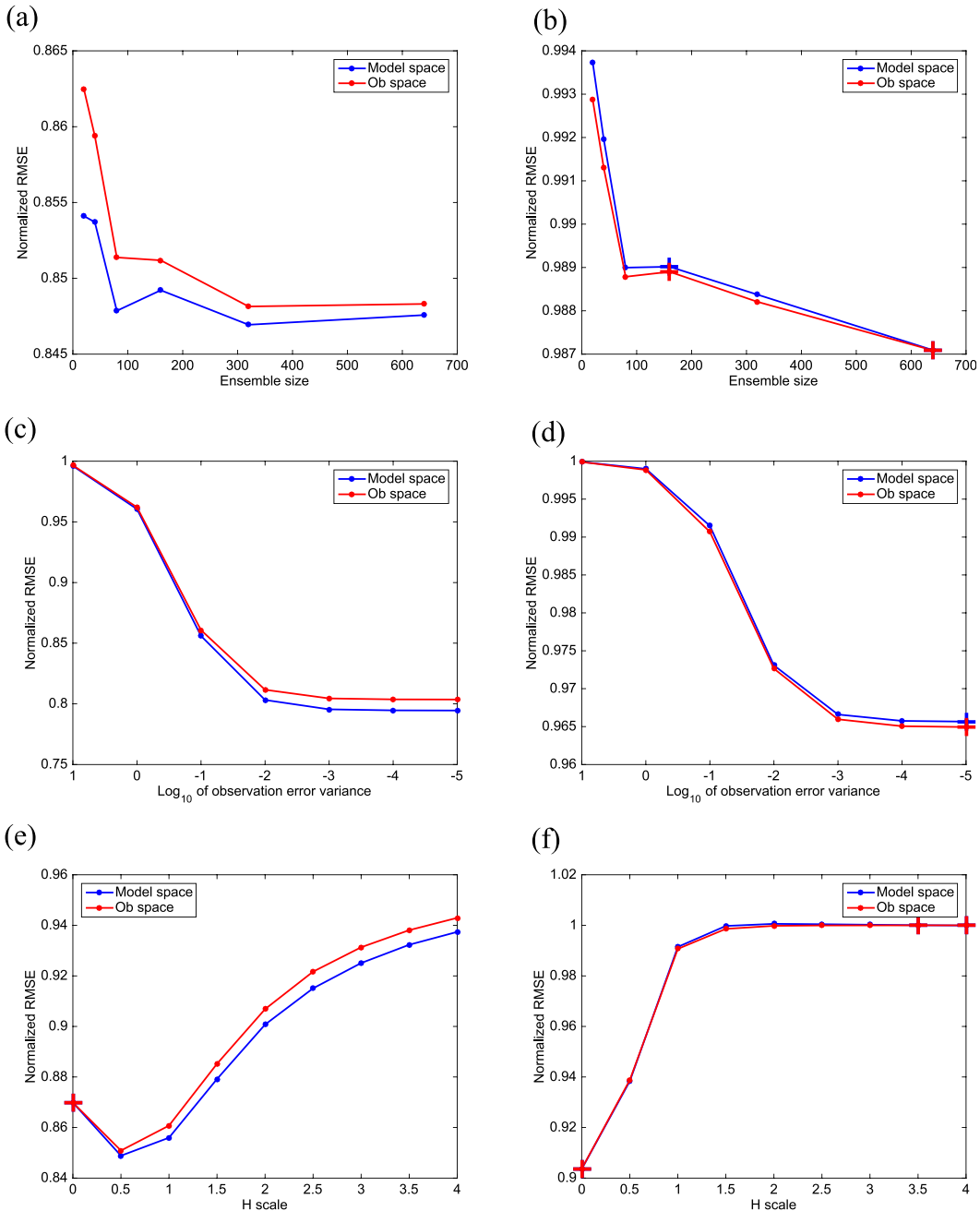

FIG. 5. The maximum analysis RMSE reduction (minimum analysis RMSE divided by the forecast RMSE) from model space and observation space localizations for (left) Gaussian $\mathbf{P}^f$ and (right) the second derivative of Gaussian $\mathbf{P}^f$ with (a),(b) varying ensemble size; (c),(d) $\mathbf{R}$; and (e),(f) scale of $\mathbf{H}$. The crosses denote situations in which the difference between model space and observation space localization is not significant at the 95% confidence level (using a paired sample t test).

localization scale 2.5, while model space localization produces the minimum error 0.9758 at localization scale 3.3. Model space localization has an error maximum at a localization scale of 0.6, and at this localization scale the error difference between model space and observation space localizations is the largest. This is due to the elimination of negative correlations in $\mathbf{P}^f$ by the model space localization, before the application of $\mathbf{H}^{\mathrm{T}}$. When the localization scale is large (>5.0), similar errors are obtained with localizations in model and observation space for the both types of true error covariances. As long as the localization scale is much larger than the

scale of the true $\mathbf{P}^f$ and $\mathbf{H}$, there is no significant loss of information from localization, regardless of whether localization is performed in model or observation space.

Figure 5 shows the maximum RMSE reduction (minimum analysis RMSE divided by the forecast RMSE) from localization in model and observation space with varying ensemble size, $\mathbf{R}$, and scale of $\mathbf{H}$. Previous results (Fig. 4) generally hold when the parameters are varied: model space localization produces larger error reduction than observation space localization when $\mathbf{P}^f$ is positive and vice versa when $\mathbf{P}^f$ contains negative values. With $\mathbf{P}^f$ as the second derivative of Gaussian, model space and observation space localizations produce similar errors for large ensembles (size 640) and large $\mathbf{R}$ ($\geq$1.0), as shown in Figs. 5b and 5d. When the scale of $\mathbf{H}$ is extremely small, that is, the radiance observation is nearly local, similar errors are obtained with localization in model and observation space (Figs. 5e, f). When $\mathbf{P}^f$ is the second derivative of Gaussian, model and observation space localization perform similarly when the scale of $\mathbf{H}$ is small ($<$1.0) and large ($>$2.0). Figures 4 and 5 suggest that model space and observation space localizations converge as ensemble size, $\mathbf{R}$, and localization length scales increase, regardless of the structure of $\mathbf{P}^f$.

5. Conclusions

Because the concept of a vertical location of satellite radiances are not well defined, observation space localization for radiance observations is not as straightforward as model space localization. However, observation space localization is used in most EnKF algorithms, since it does not require direct computation of the background-error covariance matrix. To understand the difference between model space and observation space localization, a single real radiance observation experiment and an idealized 1D model with a nonlocal $\mathbf{H}$ operator are investigated. The background-error covariances can have negative values. Results from the single radiance observation experiment show that the analysis increment with observation space localization is always smaller than that without localization and has the same sign; however, the increment with model space localization can be larger than that without localization and can change sign. Although the study of Campbell et al. (2010) suggested that observation space localization was inferior to model space localization, results from the 1D idealized model demonstrate that observation space localization can be superior to model space localization when the background-error covariance has the opposite sign of $\mathbf{H}$. However, model space and observation space localizations produce similar results with increasing ensemble size and localization length scales. This suggests that large ensemble sizes and vertical localization length scales may be the most straightforward way to ensure effective assimilation of radiance observations.

For a serial EnKF, (3) can be solved by assimilating observations one by one or in batches, which leads to slight difference of the RMSE compared to directly solving (3), but does not qualitatively change the comparison between model space and observation space localization (not shown). For satellite radiances whose vertical locations are not well defined, the choice of observation location has an impact on the observation space localization but not on the model space localization. Slightly different errors are obtained with observation space localization when the observation location is shifted, however, the general conclusions presented here still hold.

Acknowledgments. Thanks to Thomas Hamill and Haidao Lin for helpful discussions, and thanks to three anonymous reviewers for insightful comments. This work is sponsored by the NOAA High-Impact Weather Prediction Project (HIWPP) under Award NA14OAR4830123.

REFERENCES

Anderson, J. L., 2007: An adaptive covariance inflation error correction algorithm for ensemble filters. *Tellus*, **59A**, 210–224, doi:10.1111/j.1600-0870.2006.00216.x.

——, 2012: Localization and sampling error correction in ensemble Kalman filter data assimilation. *Mon. Wea. Rev.*, **140**, 2359–2371, doi:10.1175/MWR-D-11-00013.1.

——, and L. Lei, 2013: Empirical localization of observation impact in ensemble Kalman filters. *Mon. Wea. Rev.*, **141**, 4140–4153, doi:10.1175/MWR-D-12-00330.1.

Bishop, C. H., and D. Hodyss, 2009a: Ensemble covariances adaptively localized with ECO-RAP. Part 1: Tests on simple error models. *Tellus*, **61A**, 84–96, doi:10.1111/j.1600-0870.2008.00371.x.

——, and ——, 2009b: Ensemble covariances adaptively localized with ECO-RAP. Part 2: A strategy for the atmosphere. *Tellus*, **61A**, 97–111, doi:10.1111/j.1600-0870.2008.00372.x.

Buehner, M., P. L. Houtekamer, C. Charette, H. L. Mitchell, and B. He, 2010a: Intercomparison of variational data assimilation and the ensemble Kalman filter for global deterministic NWP. Part I: Description and single-observation experiments. *Mon. Wea. Rev.*, **138**, 1550–1566, doi:10.1175/2009MWR3157.1.

——, ——, ——, ——, and ——, 2010b: Intercomparison of variational data assimilation and the ensemble Kalman filter for global deterministic NWP. Part II: One-month experiments with real observations. *Mon. Wea. Rev.*, **138**, 1567–1586, doi:10.1175/2009MWR3158.1.

Burgers, G., P. J. van Leeuwen, and G. Evensen, 1998: Analysis scheme in the ensemble Kalman filter. *Mon. Wea. Rev.*, **126**, 1719–1724, doi:10.1175/1520-0493(1998)126<1719:ASITEK>2.0.CO;2.

Campbell, W. F., C. H. Bishop, and D. Hodyss, 2010: Vertical covariance localization for satellite radiances in ensemble Kalman filters. *Mon. Wea. Rev.*, **138**, 282–290, doi:10.1175/2009MWR3017.1.

Chen, Y., and D. S. Oliver, 2010: Cross-covariances and localization for EnKF in multiphase flow data assimilation. *Comput. Geosci.*, **14**, 579–601, doi:10.1007/s10596-009-9174-6.

Collard, A. D., and A. P. McNally, 2009: The assimilation of infrared atmospheric sounding interferometer radiances at ECMWF. *Quart. J. Roy. Meteor. Soc.*, **135**, 1044–1058, doi:10.1002/qj.410.

Derber, J. C., and W.-S. Wu, 1998: The use of TOVS cloud-cleared radiances in the NCEP SSI analysis system. *Mon. Wea. Rev.*, **126**, 2287–2299, doi:10.1175/1520-0493(1998)126<2287:TUOTCC>2.0.CO;2.

Emerick, A., and A. Reynolds, 2011: Combining sensitivities and prior information for covariance localization in the ensemble Kalman filter for petroleum reservoir applications. *Comput. Geosci.*, **15**, 251–269, doi:10.1007/s10596-010-9198-y.

Evensen, G., 1994: Sequential data assimilation with a nonlinear quasi-geostrophic model using Monte Carlo methods to forecast error statistics. *J. Geophys. Res.*, **99**, 10 143–10 162, doi:10.1029/94JC00572.

Fertig, E. J., B. R. Hunt, E. Ott, and I. Szunyogh, 2007: Assimilating non-local observations with a local ensemble Kalman filter. *Tellus*, **59A**, 719–730, doi:10.1111/j.1600-0870.2007.00260.x.

Gaspari, G., and S. E. Cohn, 1999: Construction of correlation functions in two and three dimensions. *Quart. J. Roy. Meteor. Soc.*, **125**, 723–757, doi:10.1002/qj.49712555417.

Hamill, T. M., J. S. Whitaker, and C. Snyder, 2001: Distance-dependent filtering of background-error covariance estimates in an ensemble Kalman filter. *Mon. Wea. Rev.*, **129**, 2776–2790, doi:10.1175/1520-0493(2001)129<2776:DDFOBE>2.0.CO;2.

Han, Y., F. Weng, Q. Liu, and P. van Delst, 2007: A fast radiative transfer model for SSMIS upper atmosphere sounding channels. *J. Geophys. Res.*, **112**, D11121, doi:10.1029/2006JD008208.

Houtekamer, P. L., and H. L. Mitchell, 1998: Data assimilation using an ensemble Kalman filter technique. *Mon. Wea. Rev.*, **126**, 796–811, doi:10.1175/1520-0493(1998)126<0796:DAUAEK>2.0.CO;2.

——, and ——, 2001: A sequential ensemble Kalman filter for atmospheric data assimilation. *Mon. Wea. Rev.*, **129**, 123–137, doi:10.1175/1520-0493(2001)129<0123:ASEKFF>2.0.CO;2.

——, and ——, 2005: Ensemble Kalman filtering. *Quart. J. Roy. Meteor. Soc.*, **131**, 3269–3289, doi:10.1256/qj.05.135.

——, ——, G. Pellerin, M. Buehner, M. Charron, L. Spacek, and B. Hansen, 2005: Atmospheric data assimilation with the ensemble Kalman filter: Results with real observations. *Mon. Wea. Rev.*, **133**, 604–620, doi:10.1175/MWR-2864.1.

Hunt, B. R., E. J. Kostelich, and I. Szunyogh, 2007: Efficient data assimilation for spatiotemporal chaos: A local ensemble transform Kalman filter. *Physica D*, **230**, 112–126, doi:10.1016/j.physd.2006.11.008.

Kang, J.-S., E. Kalnay, J. Liu, I. Fung, T. Miyoshi, and K. Ide, 2011: "Variable localization" in an ensemble Kalman filter: Application to the carbon cycle data assimilation. *J. Geophys. Res.*, **116**, D09110, doi:10.1029/2010JD014673.

Le Marshall, J., and Coauthors, 2006: Improving global analysis and forecasting with AIRS. *Bull. Amer. Meteor. Soc.*, **87**, 891–894, doi:10.1175/BAMS-87-7-891.

McCarty, W., G. Jedloveck, and T. L. Miller, 2009: Impact of the assimilation of Atmospheric Infrared Sounder radiance measurements on short-term weather forecasts. *J. Geophys. Res.*, **114**, D18122, doi:10.1029/2008JD011626.

McNally, A. P., P. D. Watts, J. A. Smith, R. Engelen, G. A. Kelly, J. N. Thepaut, and M. Matricardi, 2006: The assimilation of AIRS radiance data at ECMWF. *Quart. J. Roy. Meteor. Soc.*, **132**, 935–957, doi:10.1256/qj.04.171.

Miyoshi, T., and Y. Sato, 2007: Assimilating satellite radiances with local ensemble transform Kalman filter (LETKF) applied to the JMA global model (GSM). *SOLA*, **3**, 37–40, doi:10.2151/sola.2007-010.

——, S. Yamane, and T. Enomoto, 2007: Localizing the error covariance by physical distance within a local ensemble transform Kalman filter (LETKF). *Sci. Online Lett. Atmos.*, **3**, 89–92.

Ott, E., and Coauthors, 2004: A local ensemble Kalman filter for atmospheric data assimilation. *Tellus*, **56A**, 415–428, doi:10.1111/j.1600-0870.2004.00076.x.

Wang, X., D. Barker, C. Snyder, and T. M. Hamill, 2008: A hybrid ETKF–3DVAR data assimilation scheme for the WRF model. Part I: Observing system simulation experiment. *Mon. Wea. Rev.*, **136**, 5116–5131, doi:10.1175/2008MWR2444.1.

Weng, F., 2007: Advances in radiative transfer modeling in support of satellite data assimilation. *J. Atmos. Sci.*, **64**, 3799–3807, doi:10.1175/2007JAS2112.1.

Whitaker, J. S., G. P. Compo, X. Wei, and T. M. Hamill, 2004: Reanalysis without radiosondes using ensemble data assimilation. *Mon. Wea. Rev.*, **132**, 1190–1200, doi:10.1175/1520-0493(2004)132<1190:RWRUED>2.0.CO;2.

Zhen, Y., and F. Zhang, 2014: A probabilistic approach to adaptive covariance localization for serial ensemble square root filters. *Mon. Wea. Rev.*, **142**, 4499–4518, doi:10.1175/MWR-D-13-00390.1.

Zhou, Y., D. McLaughlin, D. Entekhabi, and G. C. Ng, 2008: An ensemble multiscale filter for large nonlinear data assimilation problems. *Mon. Wea. Rev.*, **136**, 678–698, doi:10.1175/2007MWR2064.1.